International Journal of Modelling and Simulation, Vol. 26, No. 1, 2006

AN ADVANCED VOF ALGORITHM FOR OIL BOOM DESIGN

J. Fang* and K.-F.V. Wong**

Abstract

In this paper, an accurate interface convection technique based on the volume-of-fluid (VOF) scheme is presented and the concepts of interface basis and three types of fluxes are introduced to handle two-layer fluid flow in complex geometric situations. The scheme was tested and the results proved to be accurate. We then compared the computational simulation and the laboratory experiment of an innovative boom arrangement. Satisfactory results indicate the potential for using the computational technique developed in this paper to aid in oil boom design as well as in other multilayer immiscible flow applications.

Key Words

VOF algorithm, immiscible flow, interface, oil boom

Nomenclature

C_1, C_2, C_3	= oil collection zone
ρ_{oil}, ρ_{water}, ρ_{oil}	= density
μ_{oil}, μ_{water}, μ_{oil}	= dynamic viscosity
p	= pressure
u_i	= velocity component in direction x_i
t	= time
f	= volume fraction of oil
δ_{ij}	= Kronecker delta
Re, Fr	= Reynolds number, Froude number
D_f, L_f, V_f	= flux
V_d, V_{oil}	= dark fluid volume, volume of oil
δ_{m}	= global velocity divergence

1. Introduction

With billions of gallons of oil being transferred and stored throughout the world, the potential for an oil spill is significant. The inevitability of such spills and the need to minimize environmental damage make it worth developing effective and easy-to-apply oil slick collection methods. The most common equipment used for controlling oil spills is the oil boom. Booms are used to contain the oil and keep it from spreading prior to various oil removal techniques. In an effort to achieve high oil collection efficiency, researchers have investigated boom arrangement [1–4]. Such studies are especially useful to oil spill recovery at inlets, rivers, and canals.

The purpose of this paper is to establish a computational method to test the performance of designed boom systems. Oil and water are immiscible fluids and are separated by an interface. Across the interface, the fluid density and viscosity change dramatically. Because the moving interface is highly coupled with fluid flows, the location of the interface cannot be known in advance, and it becomes an important part of the solution of this kind of hydrodynamic system. A variety of methods are available to handle the moving interfaces. Essentially, they can be classified into two categories, the Eulerian or the Lagrangrian methods. Lagrangrian methods, such as boundary integral techniques [5, 6], finite element methods [7, 8], and boundary-fitted coordinates [9, 10], maintain the interface as a discontinuity and explicitly track its evolution. No modelling is necessary to define the interface, but it is difficult for Lagrangrian methods to handle large interface deformation as well as interface folding and merging. Eulerian methods have the potential for handling large interface deformations. In these methods, the interfaces are not explicitly tracked out but are reconstructed from the properties of appropriated field variables. Among them, the Level-Set Method [11, 12] uses a distance function, and Marker-and-Cell (MAC) [13, 14] and volume-of-fluid (VOF) makes use of a fluid volume fraction variable. Level-Set Method can be easy to use in three-dimensional problems, but its interface has a finite thickness, which is artificially assigned, and the mass conservation is not guaranteed. The MAC method involves Eulerian flow field calculation and Lagrangrian liquid-particle movement. The velocity of a marker particle is found by taking the average of the Eulerian velocity in its vicinity. The average velocity field cannot be divergence-free again. Therefore, the MAC method may create high or low marker number densities in the cells. VOF method is not susceptible to the problems

**Department of Mechanical Engineering, University of Miami, Coral Gables, FL 33124, USA; e-mail: kwong@miami.edu
Recommended by Dr. I. Tansel
(paper no. 205-4148)

that may be encountered when using the Level-Set or MAC methods, but VOF methods become very complicated in three-dimensional applications. Two further major problems arise for every VOF-based algorithm. One is how to reconstruct the exact interface geometry, and the other is how to convect the interface.

We will first review some typical techniques for interface reconstruction by VOF method. The earlier and well-known technique is donor-acceptor technique [15]. The orientation of an interface segment in a cell is assumed to be either horizontal or vertical. This is the so-called zeroth-order method. To improve the accuracy of interface reconstruction, Youngs [16] and Ashgriz and Poo [17] used a sloped line in each interface cell rather than a horizontal or vertical line. The detailed method for calculating the slope was described in FLAIR [17]. Recently, Kim [18] developed a second-order model in which a second-order linear curve fits the volume fraction distribution in a block of 3×3 cells, with the interface cell in the centre of this block. A high-order model for interface reconstruction makes the high-order VOF algorithm possible. Unfortunately, in most current literature, the volume fraction convection schemes are treated simply. Therefore the total volume of one fluid is not conservative, and in some cells the volume fraction may be greater than unity or less then zero, which is physically impossible. In this paper, we developed an accurate and conservative algorithm for the volume fraction convection.

The remainder of this paper is arranged as follows. Section 2 presents the configuration of a boom system and the formulations of this problem. Numerical methods and procedure are described in Section 3. The volume fraction convection algorithm is also specified in this section. Results and discussion are given in Section 4, and the final section gives conclusions.

2. Formulation of the Problem

2.1 Configuration of the Tested Design

A cross-sectional view of a newly designed boom system by Wong and Kusijanovic [4] is illustrated in Fig. 1. On the upstream is a ramp boom with an attack angle of 15°. Following the ramp boom there are three regular booms. Between these booms are oil collection zones (C_1, C_2, and C_3). The dimensionless lengths in Fig. 1 are scaled by the depth of the regular boom, such as boom A. The width of the booms arranged in z direction is usually the same as the span of the protection area, which is much longer than the depth of the booms. So it is reasonable to reduce this problem to a two-dimensional problem.

2.2 Governing Equations

Suppose the velocity can be considered continuous across the interface, and the interface tension can be ignored due to the high Weber number in the experiment [4]. The conservation equations of mass and momentum for this two-layer flow can be written as:

mass equation

$$\rho_{,t} + (\rho u_i)_{,i} = 0 \tag{1}$$

momentum equation

$$\rho u_{i,t} + \rho u_i u_{j,j} = -p_{,i} - \rho g \delta_{i2} + (\mu u_{i,j})_{,j} \tag{2}$$

where $i, j = 1, 2$, and u_i is the velocity component in the x_i ($x_1 = x,\ x_2 = y$) direction, t is time, p pressure, ρ density, μ dynamic viscosity, g gravity, and δ_{ij} the Kronecker delta. The density and dynamic viscosity are supposed to be linear to the volume fraction f [19]:

$$\begin{aligned} \rho &= (1 - f) \cdot \rho_{\text{water}} + f \cdot \rho_{\text{oil}} \\ \mu &= (1 - f) \cdot \mu_{\text{water}} + f \cdot \mu_{\text{oil}} \end{aligned} \tag{3}$$

The definition of volume fraction f is the volume ratio of oil in a small space element. In VOF code, the small space elements are the computational cells, $f = V_{\text{oil}}/(\Delta x \cdot \Delta y)_{\text{cell}}$. The conservation of oil subjects the volume fraction f to the conservation law.

$$f_{,t} + u_i f_{,i} = 0 \tag{4}$$

It is convenient to use the following dimensionless variables, which can be obtained by choosing water density ρ, water dynamic viscosity μ_{water}, the draft L of regular boom A, and uniform upstream velocity U_0 as a dimensionally independent set of variables:

$$\begin{aligned} &\bar{x}_i = \frac{x_i}{L}, \quad \bar{t} = \frac{tU_0}{L}, \quad \bar{u}_i = \frac{u_i}{U_0}, \quad \bar{p} = \frac{p}{\rho_{\text{water}} U_0^2}, \\ &\bar{\rho} = \frac{\rho}{\rho_{\text{water}}}, \quad \bar{\mu} = \frac{\mu}{\mu_{\text{water}}} \end{aligned} \tag{5}$$

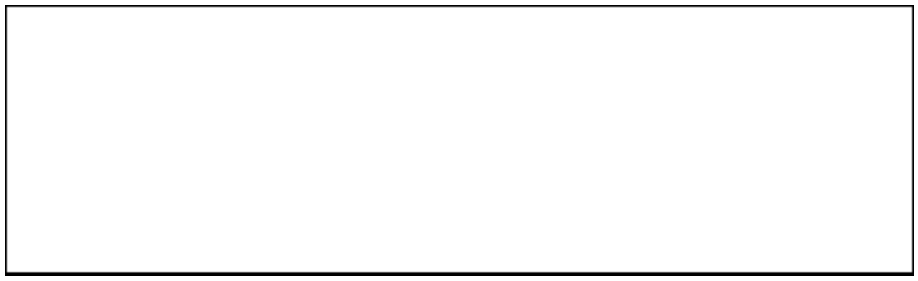

Figure 1. The configuration of the innovative boom arrangement.

After dropping the bars, the dimensionless governing equations become:

$$u_{i,i} = 0 \tag{6}$$

$$\rho u_{i,t} + \rho u_i u_{j,j} = -p_{,i} + \frac{1-\rho}{\mathrm{Fr}^2}\delta_{i2} + \frac{1}{\mathrm{Re}}(\mu u_{i,j})_{,j} \tag{7}$$

$$\begin{aligned} \rho &= 1 - f + f\rho_{\mathrm{oil}} \\ \mu &= 1 - f + f\mu_{\mathrm{oil}} \end{aligned} \tag{8}$$

$$f_{,t} + u_i f_{,i} = 0 \tag{9}$$

where Reynolds number, $\mathrm{Re} = \rho_{\mathrm{water}} U_0 L/\mu_{\mathrm{water}}$, Froude number, $\mathrm{Fr} = U_0/\sqrt{gL}$. Mass conservation equation (6) can be derived from equations (1), (3), and (4).

The computational domain is showed in Fig. 1. The incoming flow conditions are given by $u_1 = 1$, $u_2 = 0$. The outlet conditions are given as $p =$ constant and $u_{1,1} = u_{2,1} = 0$. In our computational cases, the free surface is approximated by a rigid free-slip wall; then $u_{1,2} = u_2 = 0$. On the bottom, rigid nonslip wall condition is used, $u_1 = u_2 = 0$.

As the initial condition at $t = 0$, the fluid is assumed stationary and the pressure is static. When dimensionless time $0 \le t \le 1$, we disable the VOF process and just calculate the flow field. The entrance velocity increases linearly with the time until the dimensionless velocity $u_1 = 1$. When $t > 1$, the entrance velocity is kept at 1, and the VOF begins to update the volume fraction field.

3. Numerical Method and Procedure

In VOF schemes, the volume fraction variable f is used to reconstruct and convect the interface. An accurate VOF scheme needs a correct and divergence-free velocity field, an accurate interface reconstruction technique, and an accurate convection scheme of volume fraction f. We use the SIMPLER [20] scheme to solve the N-S equations. Compared with the SIMPLE scheme, SIMPLER has a faster convergence rate, which is desired by unsteady flow calculation. The SIMPLER scheme is a finite-volume scheme. The velocities are defined on the boundaries of the volume cell. Thus VOF can use the exact velocities directly instead of the interpolation ones. The last step in SIMPLER is to correct the velocity field. In our computations, we have triply corrected the velocity in each iteration cycle to ensure a divergence-free velocity field.

The interface reconstruction scheme used in this work is rooted in the FLAIR method, with some modifications made by the authors. The main four steps taken in the present scheme are:

Step 1. Mark the cell type. Every cell is marked by one of the following three types. If $f = 0$, this cell is marked as light cell (water is called light fluid in this section); if $0 < f < 1$, this cell is marked as interface cell; in case of $f = 1$, if one of its neighbour cells satisfies $f = 0$, this cell is an interface cell, and otherwise is a dark cell (oil, the dark fluid).

Step 2. Find the interface basis and slope in an interface cell. Before calculating the slope of the interface segment in a cell, the interface basis should be determined by inspecting the volume fraction f distribution in its vicinity area. The basis is on one side of the interface cell; if we turn the basis to the bottom, the dark fluid is laid above the basis, and the angle from the basis crossing the dark fluid to the interface is an acute angle. The area is a block of 3×3 cells if all the interface sides are not laid on a solid surface or a free surface (Fig. 2(a)), or it is a block of 2×3 cells if one side is impermeable (Fig. 2(b)). If a cell has two impermeable sides, we use a simple treatment.

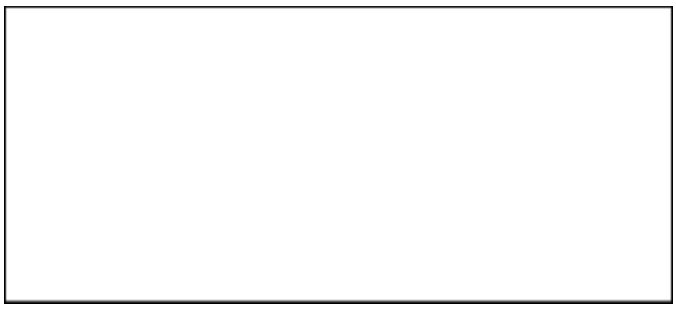

Figure 2. Determining the basis of an interface cell. The dashed line indicates the possible basis.

Consider the case showed in Fig. 2(a). We determine the interface basis by comparing the four average volume fractions.

$$f_N = \frac{1}{h_x}\sum_{k=-1}^{1} f(i+k, j-1)\cdot dx(i+k) \tag{10}$$

$$f_S = \frac{1}{h_x}\sum_{k=-1}^{1} f(i+k, j+1)\cdot dx(i+k) \tag{11}$$

$$f_W = \frac{1}{h_y}\sum_{k=-1}^{1} f(i-1, j+k)\cdot dy(j+k) \tag{12}$$

$$f_E = \frac{1}{h_y}\sum_{k=-1}^{1} f(i+1, j+k)\cdot dy(j+k) \tag{13}$$

where $f(i,j)$ is volume fraction f in cell (i,j), and $h_x = \sum_{k=-1}^{1} dx(i+k)$, $h_y = \sum_{k=-1}^{1} dy(j+k)$. If $f_P = \max(f_N, f_S, f_W, f_E)$, $P \in (N, S, W, E)$, then the side P is the basis. Actually, a common interface cell as showed in Fig. 2(a) may have two suitable bases. They are side W and S in this particular case. Therefore, when one side of an interface cell is on the solid boundary or on the free surface, at least one basis is still available from the other three sides (side N in case of Fig. 2(b)).

If two sides of an interface cell are impermeable, the flux directions on the other two sides must be opposed, from one side into the cell and from the other out. In this case, the donor–acceptor scheme is used to reconstruct and

convect the interface. The basis is set to parallel to the out-velocity direction.

If we make a rotation and let the interface stand above the basis, we can use FLAIR algorithm to calculate the slope of the interface. The slope angle may be positive or negative. If it is a negative angle, we make a mirror transformation in its vicinity area. For instance, if side S in Fig. 2(a) is the basis, then the slope has a negative angle. But if we rearrange its neighbour cells by exchanging the west side and east side cells, the slope angle will be positive.

After the proper rotation and mirror transformation, the interface geometry in a cell takes the form of one of the four subcases listed in Fig. 3.

Figure 3. Four possible geometric subcases.

Step 3. Compute the fluxes. As mentioned before, the convection of volume fraction f in VOF is not directly obtained by solving equation (9). The approach is to use the geometric information of the interface and the velocities on the sides of the interface cell.

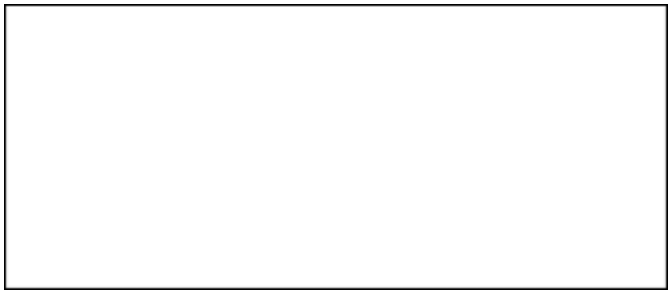

Figure 4. The convection of the volume fraction.

Most approaches found in the literature consider only the flux exchange between the interface cell and its side cell (the neighbour cell with which it shares a common side), and ignore the flux exchange between it and its corner cell (the neighbour cell with which it has an opposite corner) (see Fig. 4(a)). It is obvious that inaccuracy will result if the main fluid velocity is not parallel or vertical to the sides of cells. After every time step, one can find that the total volume of the dark fluid is changed, and in some cells, $f>1$ or $f<0$ may occur. Some of the VOF-based algorithms distribute the changed volume into cells such that the total change remains zero. This procedure artificially introduces numerical diffusion, and sometimes it causes poorer results, especially when the velocity field is complex and the number of computational steps is very large. A new approach is carried out in this study, in which every possible flux exchange has been taken into account and the exact conservation condition is naturally kept (Fig. 4(b)).

The combinations of the geometry and velocities can form many subcases. In order to handle them uniformly and efficiently, we adopt the following definitions.

- The velocity on a side is defined to be positive if it flows out the interface cell, and be negative if it flows into the interface cell.
- Three kinds of fluxes are defined for each side cell and each corner cell and all fluxes are just calculated in interface cells.
- Dark fluid volume flux flows from the interface cell to the neighbour cell, D_f.
- Light fluid volume flux flows from the interface cell to the neighbour cell, L_f.
- Total volume flux flows from the neighbour cell to the interface cell, V_f.

If any flux has a direction opposite to that of the definition, then this value is just set to zero. For a corner cell, if the velocities on its two sides have different signs, all its fluxes are zeroes. Consider the fluxes between the interface cell and SE corner cell (see Fig. 4(b)). Imagine that two steps are taken in convecting the corner fluxes, first in x direction and then in y direction. If in the first step fluxes go to the east cell from the interface cell ($u_E>0$) and then go north in the second step ($u_S<0$), no flux goes into SE cell from this interface cell (in this case, $u_E\cdot u_S<0$). But if the fluxes go south in the second step ($u_s>0$), part of fluxes that flowed into the east cell will flow into the SE corner cell (in this case, $u_E\cdot u_S>0$). Similarly, if $u_E<0$, and $u_S<0$, fluxes from SE corner cell to west will turn to the north, to the interface cell (in this case, $u_E\cdot u_S>0$), and if $u_E<0$ and $u_S>0$, no flux exchanges between SE cell and the interface cell in this circumstance ($u_E\cdot u_S<0$).

The calculation procedure is as follows:

- Calculate the side fluxes, the fluxes between the interface cell and its side cells without considering the corner fluxes.
- Calculate the corner fluxes, the fluxes between the interface cell and its corner cells.
- Update each side flux by subtracting two associated corner fluxes. For instance, each N side flux should take the NW and NE corner fluxes out.

Step 4. Update the volume fraction field. After obtaining the fluxes, we update the volume fractions of the interface cell and its all neighbour cells in the same time. Some cells may be the neighbour cells of other interface cells or the interface cells, and will then undergo further updating. The basic reason in defining fluxes is that the outgoing fluxes are known because the volume distribution in the interface cell is known. The following rules apply:

- If the neighbour cell is a dark cell, add V_f to the interface cell and subtract L_f from the neighbour cell.
- If the neighbour cell is not a dark cell, add D_f to the neighbour cell and subtract D_f from the interface cell.

Fluxes on an impermeable side *do not* need any special treatment in this step. The reason is that on this side, the velocity is zero and so are the fluxes.

4. Results and Discussion

4.1 Validation Tests

The accuracy and reliability of the numerical methods used in this work have been tested in many ways. Two global parameters are always monitored:
global velocity-divergence,

$$\delta m = \sum_{\text{all cells}} |\Delta u_1 \Delta x_2 + \Delta u_2 \Delta x_1|,$$

and total dark fluid volume,

$$V_d = \sum_{\text{all cells}} f \Delta x_1 \Delta x_2.$$

In our computations, the global velocity-divergence is controlled in less than 10^{-2}. When f is set to zero in each cell, then the problem reduces to uniform fluid case. In this way, we compared our results with Ertekin [21] at $\mathrm{Re} = 5000$ and Dennis [22] at $\mathrm{Re} = 100$. (To compare with Ertekin's results, we modified the free surface condition to nonslip boundary condition.) We found excellent agreement with both works.

To check the VOF scheme, many cases have been tested. The fluctuation of the global parameter V_d is less than 0.01% after every 1000 time steps when we apply a given divergence-free velocity field. This error is just caused by the single precision round-off error. Due to space limitations, only two tests are discussed below. To verify the results, we will suppose two fluids have the same physical properties. Case 1 is free convection of a dark-fluid circle. In this test, the velocity field is specified to be uniform, so it is exactly divergence-free. In this way, we can focus our attention on the VOF scheme itself. Different velocity orientations against the grids were tested. In Fig. 5, the original circle has a diameter of 15 cells, and the velocity field is given by $u_1 = 1,\ u_2 = -1$. After 1000 time steps, the dark circle keeps the perfect circle shape and its volume only changes 0.003%.

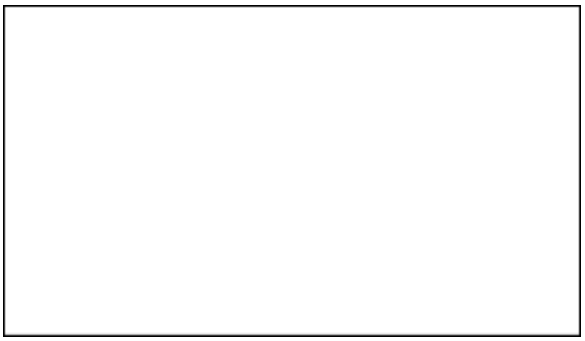

Figure 5. Free convection of a circle. Time t and total dark fluid volume V_d are dimensionless. Reference time and volume are unspecified for general case.

Case 2 is similar to a flow visualization experiment. In the upstream, three layers of dark fluid flow into the computational domain and then pass through a vertical barrier. Each layer is four cells wide at the entrance. Because two fluids have the same properties, the dark fluid does not disturb the flow and just acts as the trace ink. When the flow field reaches its steady state, the dark fluid layers should exactly follow the streamlines. In our computation, the total dark fluid volume fluctuates only 0.01% in every 1000 time steps after the flow reaches its steady state; from Fig. 6 we can see that the dark fluid layers do not show any dispersion and are confined within their streamlines, as they should be.

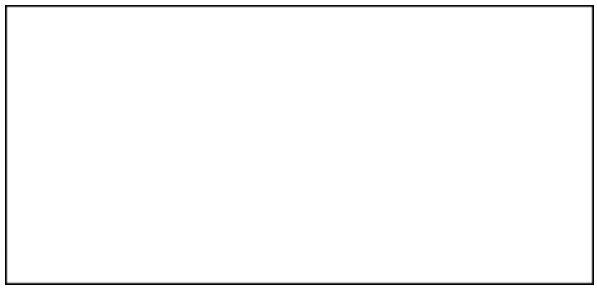

Figure 6. Three layers of dark fluid pass through a barrier ($\mathrm{Re} = 5000$). x, y are scalar space, in dimensionless form.

4.2 Numerical Study of the Oil Boom Arrangement

In the laboratory study of the boom arrangement, three velocity regimes were found [4]. When the current velocity is less than 0.2 m/s, most of the oil will stay in the front of the ramp boom. When it is greater than 0.25 m/s and less than or equal to 0.4 m/s, most of the oil can be trapped in the boom system. When the current velocity is greater than 0.5 m/s, the oil may mostly escape being trapped by the booms.

In order to compare with the experimental results, we chose our computational parameters to be the same as in the laboratory experiment. The viscosities of water and motor oil are $1.2 \times 10^{-3}\,\mathrm{N \cdot s/m^2}$ and $9.5 \times 10^{-2}\,\mathrm{N \cdot s/m^2}$, densities, $10^3\,\mathrm{kg/m^3}$ and $8.7 \times 10^2\,\mathrm{kg/m^3}$, respectively. The dimensionless oil density and viscosity are $\rho_{\mathrm{oil}} = 0.84$ and $\mu_{\mathrm{oil}} = 79$.

The draft of the boom A is 4.5 cm, and the boom arrangement is described in Fig. 1. In our computations, we have selected a grid of 181×81 to represent a rectangle domain of 30 long by 7.5 deep. The grid is not uniform in size. In the area where the oil may pass by or near the boom system, the grid is very fine. Outside those areas, the grid is asymptotically increased. The sides of the cells vary from 0.05×0.05 to 0.5×0.2.

In order to understand the function of the ramp boom, we calculate two cases for comparison. In Fig. 7, there are one-fluid streamline plots when the flow reaches its steady state condition at $\mathrm{Re} = 7725$. Fig. 7(a) is the case without a ramp boom, and Fig. 7(b) with a ramp boom. Comparing the two plots, one can deduce that the ramp helps to trap the oil in two ways. First, the ramp guides

the direction of the flow. When the fluid enters the oil collection zones, it will have a lower vertical downward velocity, and the oil will be prevented from overshooting out of these zones. Another reason is that a large quiescent oil collection zone is created by the ramp boom. As a result, in the presence of the ramp boom, the buoyant force has a longer action time to separate the fluids due to their different densities.

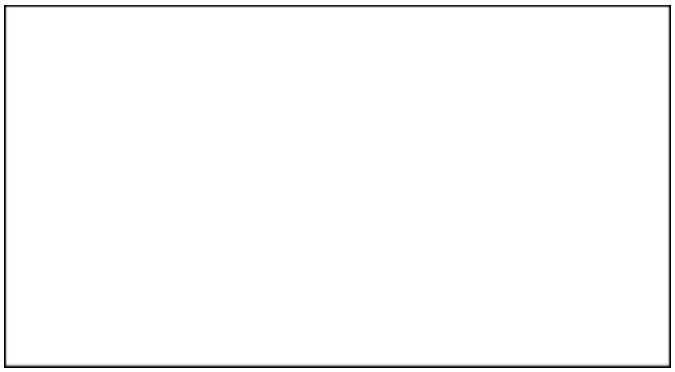

Figure 7. Streamline plots of one-fluid cases. x, y are scaled by the draft ($L = 4.5\,\mathrm{cm}$) of boom A.

Figure 8. Initial condition for the following computational cases (at $t = 0$). x, y are scaled by the draft ($L = 4.5\,\mathrm{cm}$) of boom A.

In the following section we present the computational results of several current velocities. From their definitions, Reynolds number and Froude number are directly proportional to the current velocity when other physical parameters remain unchanged: $\mathrm{Re} = 38625.0U_0$, $\mathrm{Fr} = 1.505U_0$ where U_0 is the current velocity, and it has the unit of meter per second. The initial condition is the same for each following computational case (Fig. 8).

With the current velocity $U_0 = 0.2\,\mathrm{m/s}$, the dimensionless parameters are $\mathrm{Re} = 7725$ and $\mathrm{Fr} = 0.301$. It appears from Fig. 9 that the oil inertia cannot overcome the buoyancy when it moves along the ramp boom. The oil goes forward first and then goes backward. Only a little oil enters collection zone C_1; most of the oil stays in the front of the ramp. A head wave is formed against the current in the oil layer. This head wave was also found in experimental investigation [4, 23]. Under the influence of the buoyancy, the oil has a tendency to move up and stretch out on the free surface, but the inertia of the oil and the friction between water and oil make the oil following the water current. These opposite actions cause the head wave in the front of the oil layer.

On the interface near the head wave, there is a strong shear layer. The oil may form little droplets and enter the water current owing to turbulence and Kelvin-Helmholtz effect. This is the so-called entrainment failure of oil containment by boom [24]. The entrainment failure occurs in small space and time scales; it is not included in this study.

When the current velocity increases to $0.25\,\mathrm{m/s}$, the situation is very different. All of the oil passes through the ramp boom and most of the oil is collected by zone C_1 and C_2. Fig. 10 also shows that the oil is broken into pieces and the interface is totally deformed when time is less than 30. But at time = 40, the oil stays at the top in different collection zones; the oil and water are well separated

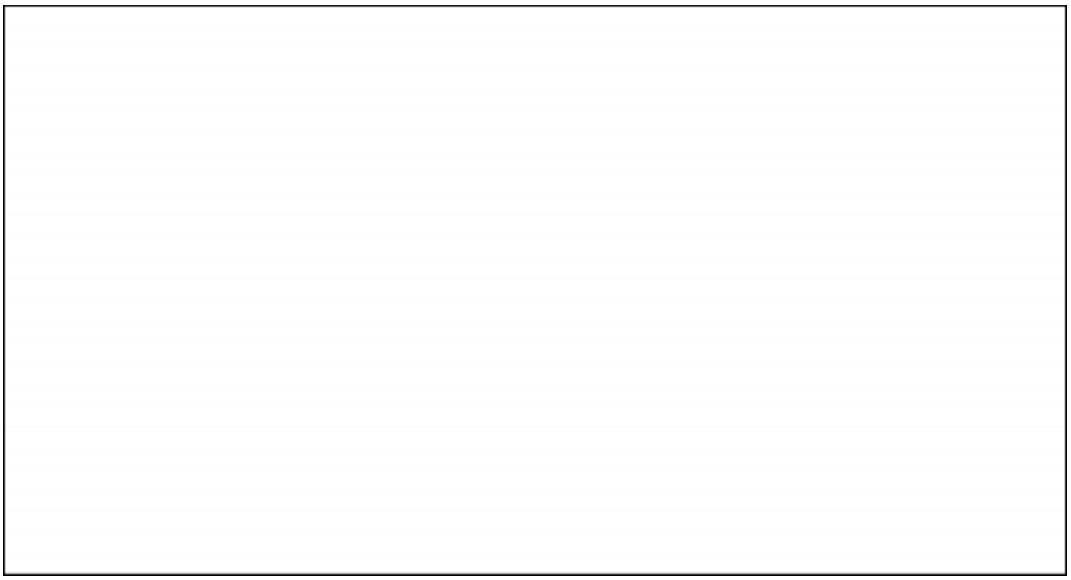

Figure 9. The oil layer evolution with current velocity of $0.2\,\mathrm{m/s}$. x, y are scaled by the draft ($L = 4.5\,\mathrm{cm}$) of boom A, and the corresponding times are $1.125\,\mathrm{s}$, $2.250\,\mathrm{s}$, $3.375\,\mathrm{s}$, $4.5\,\mathrm{s}$, $6.75\,\mathrm{s}$, and $9.0\,\mathrm{s}$, respectively.

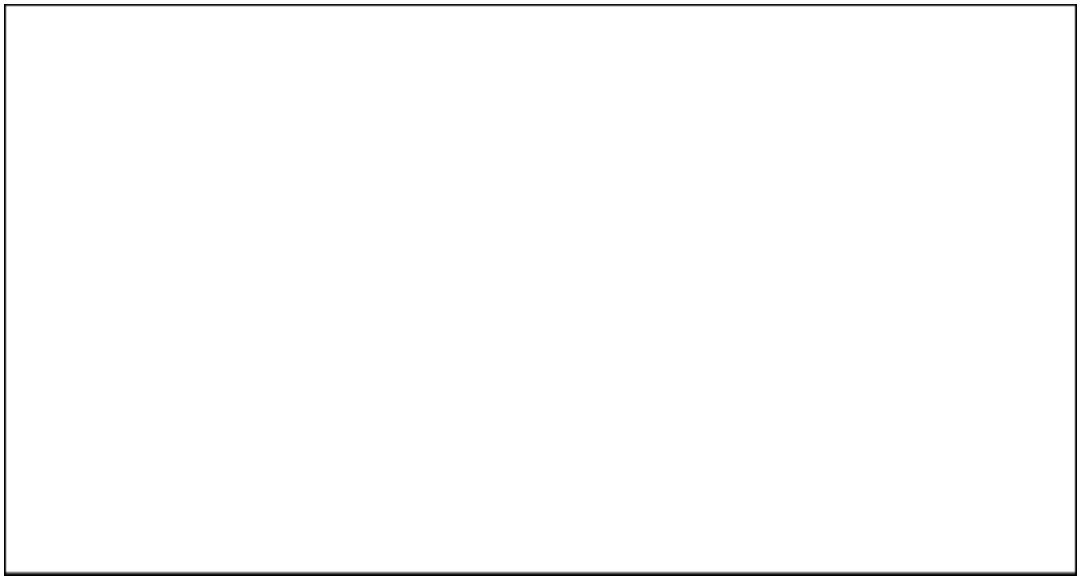

Figure 10. The oil layer evolution with current velocity of 0.25 m/s. x, y are scaled by the draft ($L = 4.5$ cm) of boom A, and the corresponding times are 0.9 s, 1.8 s, 2.7 s, 3.6 s, 5.4 s, and 7.2 s, respectively.

Figure 11. The oil layer evolution with current velocity of 0.40 m/s. x, y are scaled by the draft ($L = 4.5$ cm) of boom A, and the corresponding times are 0.5625 s, 1.125 s, 1.6875 s, 2.25 s, 3.375 s, and 5.4 s, respectively.

again. At this point, the present computational technique has handled the two-layer flow in complex geometry very well. More importantly, the criteria current velocity is quantitatively close to the experimental value, between 0.2 m/s and 0.25 m/s.

At $U_0 = 0.40$ m/s, most of the oil passes through collection zone C_1 and goes into zones C_2 and C_3 (Fig. 11). Some oil escapes from the boom system. In this computational case, the oil collection efficiency of 70% is lower than that of the experiment, which is 98% [4]. The thickness of the incoming oil layer may be one of the reasons. In the experiment, the incoming oil slick is very thin, about 0.2 mm. But in the mesh system of our numerical simulation, we cannot discretize the space that fine. When the oil layer is two grids thick initially, it is 4.5 mm thick in the experiments. It can be seen that with a thicker incoming oil layer, more oil will escape in the experiment.

More computational results are summarized in Fig. 12. The total oil volume collected by the studied boom system decreases as the current velocity increases. But in each of three separated collection zones, the oil volume has a peak value at a certain current velocity. The peak value in the last zone appears when the current velocity is near 0.4 m/s. In some sense, that oil passing through the ramp boom is similar to throwing an object under the influence of the gravity. If the shooting angle is fixed, the higher the velocity, the longer the landing distance. When this kind of landing point is on the outside of the last boom, most

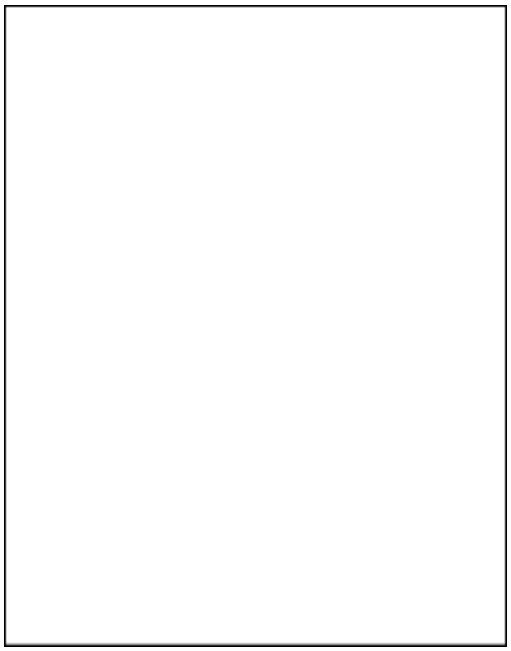

Figure 12. Oil volume collected by zones versus current velocity. Oil volume in a collection zone is the summation of $f\Delta x\Delta y$ in this zone. Total collected oil includes the oil in collection zones 1, 2, and 3, and the oil in the front of the ramp. Oil volume is in dimensionless form, scaled by $L \times L = 20.25\,\mathrm{cm}^2$ in the two-dimensional calculations.

of the oil will escape. This is the reason that the total collected oil volume decreases quickly when the current velocity exceeds 0.40 m/s.

We can then arrange the booms by a longer separated distance and find a suitable attack angle for the ramp boom to achieve a good performance. But in fact two neighbouring booms cannot be separated too widely; otherwise, the still zones will no longer exist and the collected oil will re-enter the current. Moreover, the effects of the density and viscosity of the oil and the depth of the canal make this problem much more complicated than the problem of throwing an object.

5. Conclusion

An advanced interface convection technique in complex geometry has been developed and applied to analyze an oil boom arrangement design. This technique is based on the numerical volume-of-fluid method. The volume fraction convection is conservative and accurate in nature; no additional artificial correction is necessary. The conceptual interface basis and three types of fluxes are introduced to handle the possible combinations of complex interface geometry and the velocity field. These definitions make this VOF algorithm easy to use. By using this scheme, we preliminarily studied the performance of an oil boom arrangement. Our computation shows that the ramp boom creates a flow pattern for trapping the oil slick in the oil collection zone. Three velocity regimes, which have been found in the laboratory experiments, are also found in our numerical simulations, and the critical velocities obtained from the experiment [4] and our computations agree with each other. The successful primary study shows that this VOF scheme can be used in the computer-aided boom arrangement design and in other interface applications.

References

[1] J.-M. Lo, Laboratory investigation of single floating booms and series of booms in the prevention of oil slick and jellyfish movement, *Ocean Engineering*, *23*(6), 1996, 519–531.

[2] K.V. Wong & D. Guerrero, Quantitative analysis of shoreline protection by boom arrangements, *Proc. 2nd Int. Oil Spill R&D Forum*, London, May 1995.

[3] K.V. Wong & A. Wolek, Application of flow visualization to the development of an innovative boom system, *Proc. 19th Arctic and Marine Oil Spill Program Technical Seminar*, Calgary, Canada, June 1996.

[4] K.V. Wong & I.P. Kusijanovic, Oil spill recovery methods for inlets, rivers and canals, unpublished paper, 1998.

[5] M. Natori & H. Kawarada, Numerical solution of free surface drainage problem of two immiscible fluids by the boundary element method, *Japanese Journal of Applied Physics*, *24*, 1985, 1359–1362.

[6] H.C. Henderson, M. Kok, & W.L. de Koning, Computer-aided spillway design using the boundary element method and non-linear programming, *International Journal of Numerical Mathematical Fluids*, *13*, 1991, 625–641.

[7] D.R. Lynch, Unified approach to simulation on deforming elements with application to phase change problems, *Journal of Computational Physics*, *47*, 1982, 387–411.

[8] P. Bach & O. Hassager, An algorithm for the use of the Lagrangian specification in Newtonian fluid mechanics and applications to free-surface flow, *Journal of Fluid Mechanics*, *152*, 1985, 173–190.

[9] G. Ryskin & L.G. Leal, Numerical solution of free-boundary problems in fluid mechanics, Part 1: The finite-difference technique, *Journal of Fluid Mechanics*, *148*, 1984, 1–17.

[10] N.S. Asaithambi, Computation of free-surface flows, *Journal of Computational Physics*, *73*, 1987, 380–394.

[11] S. Osher & J.A. Sethian, Fronts propagating with curvature-dependent speed: Algorithms based on Hamilton-Jacobi formulations, *Journal of Computational Physics*, *79*, 1988.

[12] M. Sussman, P. Smereka, & S. Osher, A level set approach for computing solutions to incompressible two-phase flow, *Journal of Computational Physics*, *114*, 1994.

[13] R.K.-C. Chan & R.L. Street, A computer study of finite-amplitude water waves, *Journal of Computational Physics*, *6*, 1970, 68–94.

[14] H. Miyata, Finite difference simulation of breaking waves, *Journal of Computational Physics*, *65*, 1986, 179–214.

[15] A.J. Chorin, Curvature and solidification, *Journal of Computational Physics*, *57*, 1985, 472–490.

[16] D.L. Young, Time-dependent multi-material flow with large fluid distortion, in K.W. Morton & M.J. Baineks (Eds.), *Numerical methods for fluid dynamics* (New York: Academic Press, 1982).

[17] N. Ashgriz & J.Y. Poo, FLAIR: Flux line-segment model for advection and interface reconstruction, *Journal of Computational Physics*, *93*, 1991, 449–468.

[18] S.-O. Kim & H.C. No, Second-order model for free surface convection and interface reconstruction, *International Journal for Numerical Methods in Fluids*, *26*, 1998, 79–100.

[19] E.G. Puckett, A.S. Almgren, J.B. Bell *et al.*, A high-order projection method for tracking fluid interface in variable density incompressible flows, *Journal of Computational Physics*, *130*, 1997, 269–282.

[20] S.V. Patankar, *Numerical heat transfer and fluid flow* (Washington: Hemisphere Publishing, 1979).

[21] R.C. Ertekin & H. Sundararaghavan, The calculations of the instability criterion for a uniform viscous flow past an oil boom, *Journal of Offshore Mechanics and Arctic Engineering*, *117*, 1995, 24–29.

[22] S.C.R. Dennis, O. Wang, M. Coutanceau, & J.-L. Launay, Viscous flow normal to a flat plate at moderate Reynolds numbers, *Journal of Fluid Mechanics*, *248*, 1993, 605–635.

[23] G.A.L. Delvigne, Barrier failure by critical accumulation of viscous oil, *Proc. Oil Spill Conf., USEPA, USCG, and API*, 1989, 143–148.

[24] S.T. Grilli, Z. Hu, & L.S. Malcolm, Numerical modeling of oil containment by a boom, *Proc. 19th Arctic and Marine Oil Spill Program Technical Seminar*, Calgary, Canada, 1996, 343–376.

Biographies

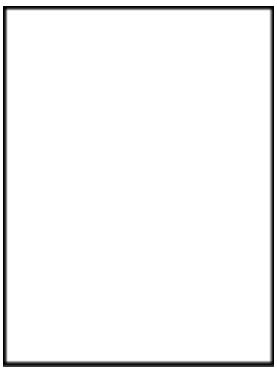

Jianzhi Fang currently works within the IT industry in the Miami area.

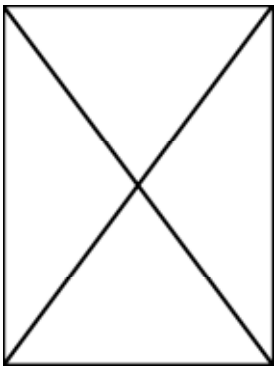

Kau-Fui Wong has been a professor for almost 26 years. In the oil spill community he is popularly known as "Dr. Boom." His research interests are energy and the environment, and recently he has developed an interest in nanotechnology.